Interface-Coupled $BiFeO_3/BiMnO_3$ Superlattices with Magnetic Transition Temperature up to 410 K

Eun-Mi Choi, Josée E. Kleibeuker, Thomas Fix, Jie Xiong, Christy J. Kinane, Darío Arena, Sean Langridge, Aiping Chen, Zhenxing Bi, Joon Hwan Lee, Haiyan Wang, Quanxi Jia, Mark G. Blamire, and Judith L. MacManus-Driscoll*

In the field of multiferroics, the coexistence of magnetism and ferroelectricity in perovskite oxides (ABO_3) has drawn increasing interest due to their potential for multifunctional devices, for example, magnetoelectric random access memory, tunable multifunctional spintronic devices including four-state memory devices, and spin filters.[1–3] Room temperature operating multiferroics are currently of intense scientific interest for these devices.[1–3] An important requirement for multiferroics is a strong coupling between the ferroic properties. Two of the most widely studied multiferroics are $BiMnO_3$ (BMO) and $BiFeO_3$ (BFO). BMO is one of the rare multiferroic materials that can possess both ferromagnetism (FM) and ferroelectricity (FE). It has a paramagnetic–ferromagnetic transition temperature (T_C) of 105 K and a magnetic saturation moment (M_S) of 3.6 Bohr magneton/formula unit (μ_B/f.u.). Unfortunately, its electrical polarization is very small (0.1 μ_C cm^{-2} at ≈90 K) or it is even paraelectric.[4] In BFO, strong FE behavior (Ferroelectric transition temperature, $T_{C,FE} \approx 1103$ K) coexists together with antiferromagnetism (AFM). BFO has an incommensurate cycloidally modulated G-type AFM structure with a large period of 62 nm (Néel temperature, $T_N \approx 650$ K).[5,6] Despite having ferroelectric and magnetic ordering at high temperatures, BFO has drawbacks for practical applications. Most notably the weak FM-like magnetic behavior results from destruction of its incommensurate magnetic structure leading to AFM.[6] With strong ferromagnetic behavior in BMO and strong ferroelectric behavior in BFO, various studies have suggested combining BMO and BFO in order to achieve room-temperature (RT) multiferroicity.[7–10]

One approach is to modify the local spin configuration of Fe by chemical doping at the *B*-site.[8,9] By 50% doping, this simple concept could result in ordered double perovskite ferrites of $Bi^{3+}{}_2Fe^{(3+n)+}TM^{(3-n)+}O^{2-}{}_6$ (TM = transition metal: Cr, Mn, Co, Ni, and Cu) giving antiferromagnetically coupled high spin state of the TM and Fe. However, this concept has not been widely realized due to the lack of cation ordering as a result of negligible differences in ionic valences and ionic radii.[11–15] On the other hand, disordered double perovskites (notably $BiFe_{0.5}Mn_{0.5}O_3$ (BFMO) and Bi_2CoMnO_6 (BCMO)) show a strongly enhanced T_C albeit with lower magnetic moment than expected for the ordered structure.[16,17]

Pálová et al. extended the idea of ordered double perovskites by theoretically studying BFMO with an ordered nanoscale checkerboard structure (NCB–BFO/BMO, see **Figure 1**a), i.e., columnar *B*-site ordering.[10] Their calculations predict that an ordered NCB–BFO/BMO would be ferroelectric and ferrimagnetic (FiM) with M_S of 3.8 μ_B/Fe–Mn pair and T_C of 406 K, as a result of magnetic ordering arising from the superexchange coupling between the neighboring AFM–Fe and FM–Mn.[10] Unfortunately, spontaneous columnar *B*-site ordering is not expected and high quality growth of artificial 1:1 BFO/BMO superlattices along the ⟨110⟩ direction is very hard.

Therefore, it is worth considering (001)-oriented BMO/BFO superlattices (SL–BFO/BMO) instead (Figure 1b). Similar to NCB–BFO/BMO, interfacial Fe–Mn ferromagnetic ordering and a concomitant increase in T_C can be expected in SL–BFO/BMO. In this structure, small local variations in magnetic behavior will also be expected since the number of Fe–Mn nearest neighbors is halved for a 1:1 SL–BFO/BMO compared to NCB–BFO/BMO.[10]

Various studies on short period perovskite superlattices have shown that the magnetic behavior can be enhanced by the interaction between the *B*-site cations. For example, Ueda et al. reported ferromagnetism at 375 and 230 K in (111)-oriented

Dr. E.-M. Choi, Dr. J. E. Kleibeuker, Dr. T. Fix, Prof. M. G. Blamire, Prof. J. L. MacManus-Driscoll
Department of Materials Science
University of Cambridge
27 Charles Babbage Road, Cambridge CB3 0FS, UK
E-mail: emc63@cam.ac.uk

Dr. J. Xiong, Dr. A. Chen, Dr. Z. Bi, Dr. Q. Jia
Center for Integrated Nanotechnologies
Los Alamos National Laboratory
Los Alamos, NM 87545, USA

Dr. J. Xiong
State Key Laboratory of Electronic Thin Films and Integrated Devices
University of Electronic Science and Technology of China
Chengdu 610054, P. R. China

Dr. C. J. Kinane, Dr. S. Langridge
ISIS, Science and Technology Facilities Council
Rutherford Appleton Laboratory
Didcot OX11 0QX, UK

Dr. D. Arena
National Synchrotron Light Source
Brookhaven National Laboratory
Upton, NY 11973, USA

Dr. D. Arena
Department of Physics
University of South Florida
Tampa, FL 33620-7100, USA

Dr. A. Chen, Dr. Z. Bi, Dr. J. H. Lee, Prof. H. Wang
Department of Electrical and Computer Engineering
Texas A&M University
College Station, TX 77843-3128, USA

The copyright line of this paper was changed 7 March 2016 after initial publication.

DOI: 10.1002/admi.201500597

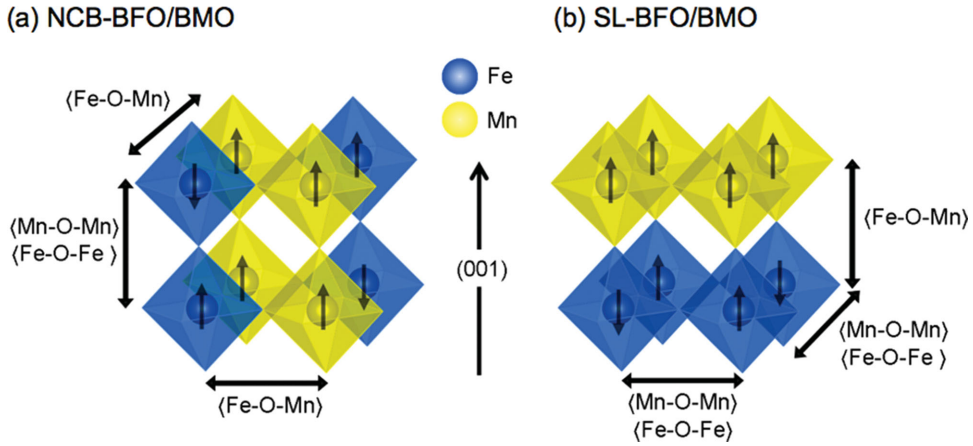

Figure 1. Schematic illustration of the BFO/BMO structure and the various possible magnetic interactions: a) (001)-oriented NCB–BFO/BMO, b) (001)-oriented SL–BFO/BMO. Arrows in octahedra indicate ordering of Fe and Mn spins. The Bi ions at the *A*-site are not shown.

1:1 $LaCrO_3/LaFeO_3$ and $LaMnO_3/LaFeO_3$ superlattices, respectively, while the parent bulk materials are AFM.[18,19] Moreover, interfacial FM has been observed at 95 and 75 K in (001)-oriented $CaMnO_3/CaRuO_3$ and $LaNiO_3/CaMnO_3$ superlattices, respectively even though $CaMnO_3$ is AFM and both $CaRuO_3$ and $LaNiO_3$ are paramagnetic.[20–22] Additional changes in the *B*-*B*′ magnetic interactions may result from internal charge transfer from *B* to *B*′.[20–24] Internal charge transfer has been observed in, e.g., (001)-oriented $LaNiO_3/LaMnO_3$ superlattices from Mn^{3+} to Ni^{3+}, similar to rock salt ordered La_2NiMnO_6.[23,24] As a result, interface-induced ferromagnetism was found in the paramagnetic $LaNiO_3$ layer. Moreover, the lattice strain from the substrate as well as the superlattice interfaces can affect the magnetic behavior as a result of changes in orbital ordering or bonding distortion of the BO_6 octahedra.[25–29]

Here, in SL–BFO_m/BMO_m (m = 1, 2, 4, and 8 unit cells (u.c.)), tuning Fe–Mn magnetic interactions through interfacial strain and charge engineering is demonstrated. Detailed analysis of both structural and magnetic features of superlattices using X-ray diffraction (XRD) and X-ray absorption spectroscopy (XAS) supports our conclusions. We show the presence of three magnetic transitions in SL–BFO/BMO. For all SL films, T_{C1} is observed at around 145 ± 15 K, which is significantly higher than the T_C of bulk BMO (≈100 K).[4] m = 1, 2 superlattices even showed ferromagnetic behavior at room temperature with a T_{C2} of ≈410 K for m = 1 and ≈320 K for m = 2, whereas m = 4, 8 showed a $T_{C,BMO}$ of 96 K which is close to bulk BMO. Recently, a spin glass was observed for BFO/BMO multilayers with m = 1.[30] These samples were suggested to be relaxed and had a single out-of-plane film lattice parameter of ≈3.93 Å which is considerably smaller than c_{pc} = 3.970 ± 0.005 Å (pc is pseudocubic), as measured for our m = 1 films, as shown later. This difference is likely the result of the use of different growth conditions since the creation of highly epitaxial in-plane strained BFO and BMO is difficult. We have found that it is necessary to carefully optimize the growth conditions to create the desired highly strained, heteroepitaxial films with strong ferrimagnetic coupling between BFO and BMO.

To verify both the epitaxy as well as the phase purity of the superlattices of this work, we measured out-of-plane XRD scans (see **Figure 2**a). The scans show that all superlattices grew epitaxially on $SrTiO_3$ (STO), showing pseudocubic $(001)_{pc}$ reflections.[31] No superlattice peaks from the multilayer were observed; however, this does not indicate the lack of a high quality SL–BFO/BMO structure since any minor interface roughening reduces the intensity of these peaks dramatically due to the small difference between scattering factors of BMO and BFO. A minor contribution of monoclinic BMO (<1%) was observed in all films. The monoclinic phase could be expected to form as a result of strain relaxation.[31] For the superlattices with m = 4, 8, a minor contribution of Bi_2O_3 was present. Note that the impurity phases were not observed by transmission electron microscopy (TEM). TEM images across the SL layers showed a single uniform structure (see inset of Figure 2a for a representative TEM image of a 1/1 SL–BFO/BMO taken around the substrate–film interface).

To investigate the out-of-plane lattice parameters in more detail, symmetric reciprocal space maps (RSMs) around STO (004) were conducted (see Figure 2b). For the short period superlattice (m = 1), a single film peak (c_{pc} = 3.970 ± 0.005 Å) corresponding to the SL–BFO/BMO was observed. The single peak indicates that the two lattices are strain coupled to give a single out-of-plane lattice parameter. The large c parameter is consistent with in-plane compression of the film lattices by the smaller STO lattice ($a_{pc–bulk}$ BMO = 3.935 Å, $a_{pc–bulk}$ BFO = 3.962 Å and a_{bulk} STO = 3.905 Å), and consequent out-of-plane elastic lattice extension of both the BMO and BFO lattices.

As indicated by the dashed lines, with increasing m a clear separation of the out-of-plane film peaks for BMO and BFO occurs. A distinct increase of the BFO out-of-plane lattice parameter was found (to c_{pc} = 3.992 ± 0.005 Å) when m increased to 8. On the other hand, for BMO only a small decrease of the out-of-plane lattice parameter occurred with increasing m (from c_{pc} = 3.970 ± 0.005 Å for m = 1 to c_{pc} = 3.950 ± 0.005 Å for m = 8). The small decrease in c_{pc} for BMO with increasing m is consistent with the BMO bulk lattice being closer to STO and hence being subject to less in-plane compression. This was explored further from asymmetric RSM scans around the STO (103) reflection which reveals both the in-plane and out-of-plane strain states in the films (Figure 2c).

In Figure 2c, the same (*H*00) positions were observed for the film and the substrate which confirmed coherent growth of the

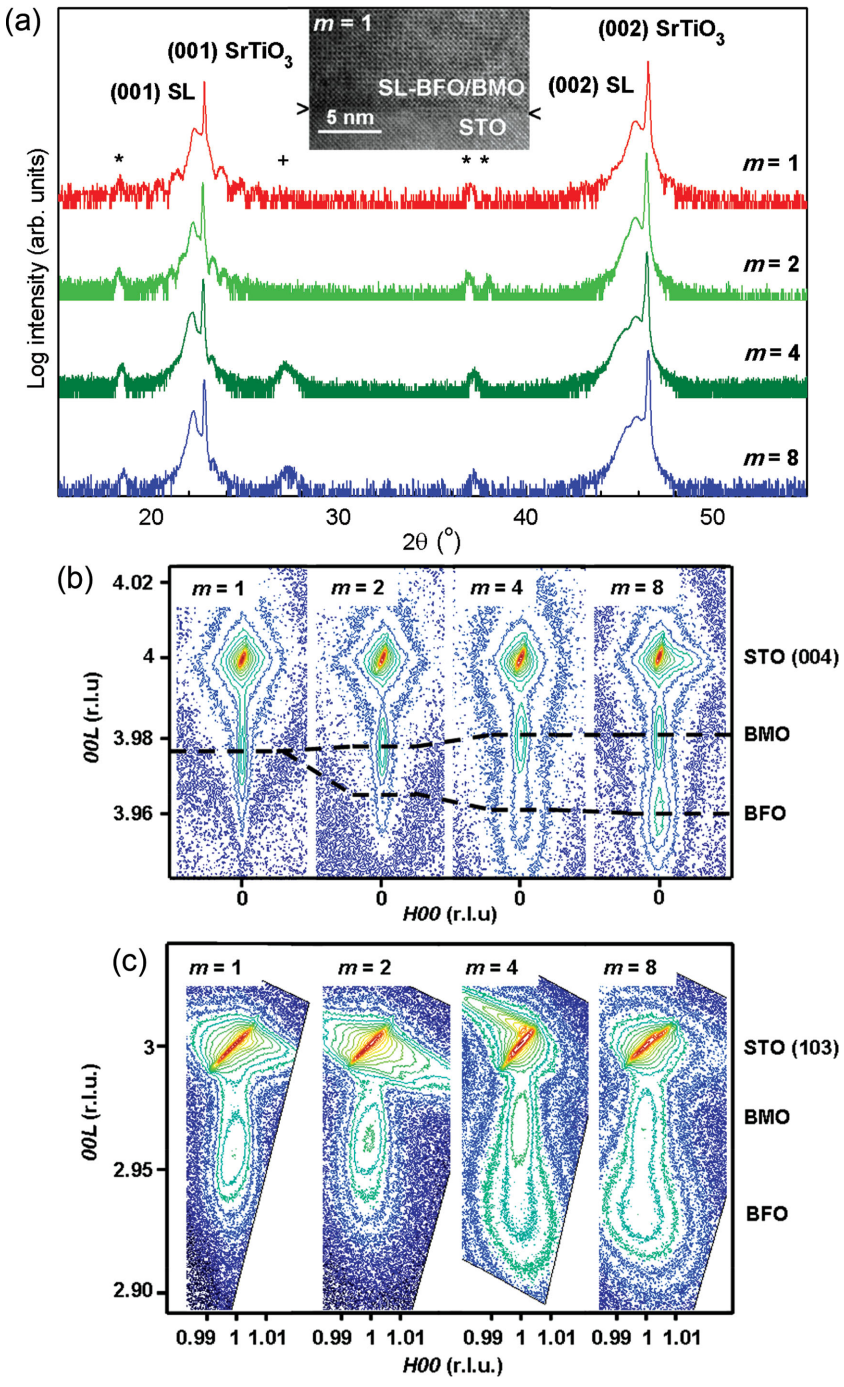

Figure 2. XRD spectra of the SL–BFO/BMO: a) Out-of-plane XRD spectra (2θ–ω scan). The BFO/BMO film peaks are labeled with SL. Additional impurity peaks corresponding to the monoclinic BMO phase and the Bi_2O_3 phase are marked by * and + respectively. The inset shows a high resolution cross-sectional TEM images in the STO ⟨100⟩ zone axis of an $m = 1$ superlattice near the SL/STO interfaces which is indicated by a bracket. b) Symmetric RSMs around the (004) reflection of STO for the $m = 1$, 2, 4 and 8 superlattices. Dashed lines show the trend in the peak positions for BMO and BFO. c) Asymmetric RSMs around the (103) reflection of STO of the $m = 1$, 2, 4 and 8 superlattices.

superlattices and full in-plane strain of both the BMO and BFO films in the superlattice structure. Interestingly, the BMO (*H0L*) peak hardly relaxed with *m*, while some peak broadening of the BFO (*H0L*) peak was observed indicating some in-plane relaxation. This means that although small changes in the BMO structure were observed, the change in tetragonal distortion (c/a) of the BMO layer was small ($c/a = 1.018$ for $m = 1$ to $c/a = 1.013$ for $m = 8$). For BFO a shift to lower reciprocal *L* value was also observed with increasing *m*, consistent with the downward shift of STO (004) reflection of Figure 2b. The results show that minor in-plane relaxation of the BFO occurs for $m = 4$, 8 and the out-of-plane lattice parameter increases toward bulk values, i.e., c_{pc} of BFO increases with *m*. The appearance of in-plane relaxation with increasing *m* indicates that the BMO/BFO interface supports BFO to maintain the strain state.[32]

To compare the magnetic properties of SL–BFO/BMO with bulk BMO, we measured the field-cooled (FC, 500 Oe) temperature dependence of the magnetic moment (*M*–*T*) for all superlattices (**Figure 3**a). To determine the transition temperature, we undertook first derivatives of the *M*–*T* curves (dM/dT). For $m = 4$ and 8, a magnetic transition is observed at 96 K (the value for bulk BMO, $T_{C,BMO}$). For all the films, a clear magnetic transition is observed at around 145 ± 15 K (T_{C1}), which is significantly higher than the T_C of bulk BMO. Interestingly, for $m = 1$, 2, a second magnetic transition is observed above room temperature (T_{C2}), at 410 K for $m = 1$, and at 320 K for $m = 2$. To determine the origin of T_{C1} and T_{C2}, we deconvoluted the *M*–*T* curves into two different transitions by using the saturation magnetic moment from the *M*–*H* loops measured at various temperatures (see Figure S1 in the Supporting Information).

From the deconvoluted *M*–*T* curves, we can deduce that the high T_{C2} for $m = 1$, 2 originates from the change of the Mn environment in BMO. The environment of Mn in BMO for $m = 1$, 2 is different to $m = 4$, 8 since BMO is directly coupled to BFO, giving a single, strained BFO–BMO lattice (Figure 2) similar to the NCB–BFO/BMO lattice (Figure 1a). T_{C1} is observed for all the films. A plot of T_{C1}, T_{C2}, and $T_{C,BMO}$ versus *m* for the various superlattices is given in the inset of Figure 3a. Figure 3b shows the relationship between T_{C1} and the out-of-plane lattice parameter of BFO.

To get a better understanding of the magnetic behavior of these superlattices, we also measured the magnetic hysteresis loops (*M*–*H*) of $m = 1$ and 8 superlattices at 10 K (Figure 3c). The M_S (at 5 T) for the $m = 1$ superlattice was found to be 90 emu cc^{-1} (≈0.59 μ_B/f.u.) whereas the M_S for the $m = 8$ was slightly lower, 80 emu cc^{-1} (≈0.52 μ_B/f.u.). The measured M_S

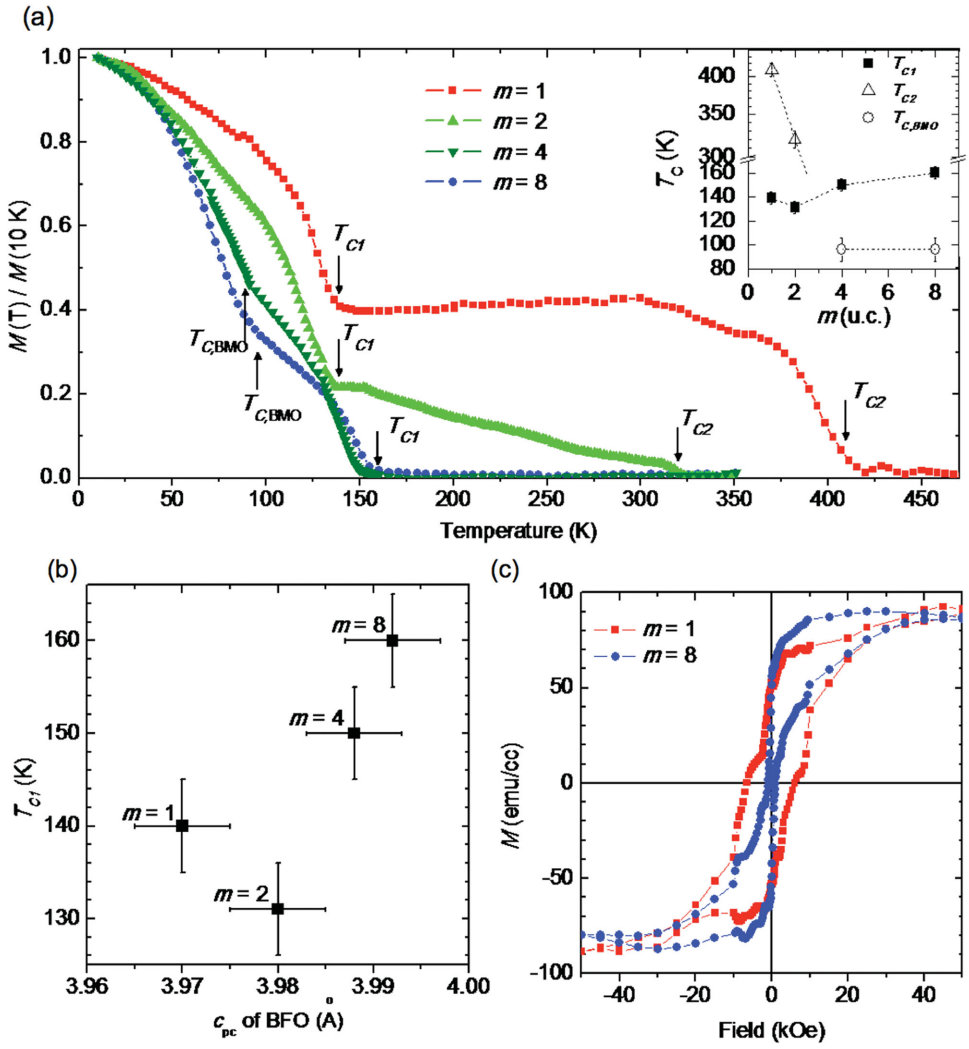

Figure 3. The magnetic properties of SL–BFO/BMO: a) Normalized in-plane FC *M*–*T* curves of superlattices with m = 1, 2, 4, and 8 at 500 Oe. Inset shows the magnetic transition temperatures, T_{C1} (black square), T_{C2} (open triangle), and $T_{C,BMO}$ (open circle), versus m. The dashed lines in the inset figure are a guide to the eye. b) The relationship between the magnetic transition temperatures, T_{C1}, and the pseudocubic out-of-plane lattice parameter of BFO. c) In-plane magnetic hysteresis (*M*–*H*) loops in the range of $-50 \leq H \leq 50$ kOe at 10 K.

values are lower than that of bare BMO films grown on STO (1.87 μ_B/f.u.) and the estimated values of antiferromagnetically ordered Fe^{3+}–O–Mn^{3+} (1 μ_B/f.u.) or ferromagnetically ordered Fe^{3+}–O–Mn^{3+} (4.5 μ_B/f.u.).[14,19,33] The lower M_S value of our superlattices is likely to be caused by complex effects resulting from a mixture of AFM and FM ordering which can arise from internal charge transfer leading to mixed ionic valences for Mn and Fe.[19] Also note that the in-plane BMO/BFO interface is present along the step edges. However, the effect of in-plane Fe–Mn interactions on the M_S of our superlattices can be expected to be within the error of the measured values as the fraction is very small compared to the fraction of out-of-plane Fe–Mn interactions («1 %).

The superlattices show an increase in coercivity (H_C) (Figure 3c) compared to bare BMO films grown on STO (H_C = 470 Oe).[33] While for the m = 8 superlattice the enhancement of H_C was doubled (H_C = 900 Oe), for the m = 1 superlattice a much more dramatic enhancement was found (H_C = 5.6 kOe). To clarify the origin of the increase of H_C, we deconvoluted the experimental *M*–*H* loops into two different transitions (loop1 and loop2, see Figure S2 in the Supporting information). A squarer and narrower loop (loop1) is simulated by subtracting a trial function of the form $M = M_S \tanh\{\alpha(H \pm H_C)\}$ from the experimental data. The residual *M*–*H* loop (loop2) is of a reasonable form and has a much higher coercivity. For the m = 8 sample, the H_Cs are 400 Oe (loop1) and 4.5 kOe (loop2), and the H_C of loop1 is close to that of plain BMO films.[33] For the m = 1 sample, the *M*–*H* loop is decomposed into two *M*–*H* curves with H_Cs of 1.2 (loop1) and 9.2 (loop2) kOe. Therefore, it seems reasonable to assume that in both cases the loop1 relates to BMO. The enhanced H_C for m = 1 can be understood by the general thickness dependence of H_C which tends to decrease with increase of magnetic layer thickness.[34,35] The broader loop2 presumably originates from a ferromagnetic BFO phase with T_{C1} of ≈145 K for which the magnetic hardness can be understood in terms of an exchange interaction between FM– and a residual AFM–BFO matrix.[36,37]

XAS near the Mn $L_{2,3}$ and Fe $L_{2,3}$ absorption edges was carried out to determine the Mn and Fe oxidation states (see **Figure 4**a,b). A clear change in the fingerprint of the Mn spectra versus m is present, indicating a variation of the oxidation state of Mn. Comparing our Mn spectra with those of simple oxides, the line shape of the $m = 8$ superlattice spectrum is close to that of Mn_2O_3, indicating a predominance of Mn^{3+}.[38,39] By decreasing m, the peak around 641 eV becomes stronger and well defined. Comparing the Mn–L edge peak shape of our $m = 1$ superlattice with those of simple oxides, the peak shape of Mn for the $m = 1$ superlattice is similar to the peak shape of Mn_3O_4, suggesting that approximately one-third of all Mn ions are filled by Mn^{2+}.[38–40]

Comparing the Fe spectra, a small change in line shape versus m is present as well. The spectrum of the $m = 8$ superlattice shows a sharp peak at ~710 eV with a clear shoulder at lower energy. This strongly suggests a predominance Fe^{3+} valence with a small fraction of Fe^{4+}.[40,41] By reducing m, the observed shoulder at lower energy is partially merged into the strong peak at 710 eV. Comparing our spectra with the literature, this change in line shape indicates an increase of Fe^{4+} concentration when reducing m.[41,42] The observed trends for Fe and Mn valence states versus m are in agreement with each other.

Summarizing the XAS results, for the $m = 1$ superlattices, we find clear mixed valence states of the B-site cations, $Fe^{3+/4+}$ and $Mn^{2+/3+}$, while for $m = 8$ superlattices we have a predominance of Fe^{3+} and Mn^{3+}, but also some Fe^{4+} and Mn^{2+} are present. This suggests that charge transfer occurs from Fe to Mn near the interface. Considering the band gaps (Δ) of both BFO and BMO, charge transfer from BFO to BMO is remarkable since Δ_{BFO} is larger than Δ_{BMO}, 2.8 and 1.6 eV respectively.[33,43] An alternative explanation for the presence of $Fe^{3+/4+}$ and $Mn^{2+/3+}$ would be leakage of electrons from the Fe–site into the BMO layer. Such leakage is predicted to be on the order of 0.07 e^-/Mn in order to stabilize interfacial FM in $CaMnO_3/CaRuO_3$, and is suggested to occur experimentally in SL of $CaRuO_3/CaMnO_3$ and $LaNiO_3/CaMnO_3$.[20–22] Note that such a leakage has only been observed when $CaRuO_3$ and $LaNiO_3$ are metallic. BFO is an insulator, but BFO films are often not highly resistive owing to the presence of defects in the structure, allowing small charge leakage. In addition, charge transfer has been suggested to occur at the interface of BFO and half-metallic $La_{0.7}Sr_{0.3}MnO_3$ to explain interface magnetism.[44]

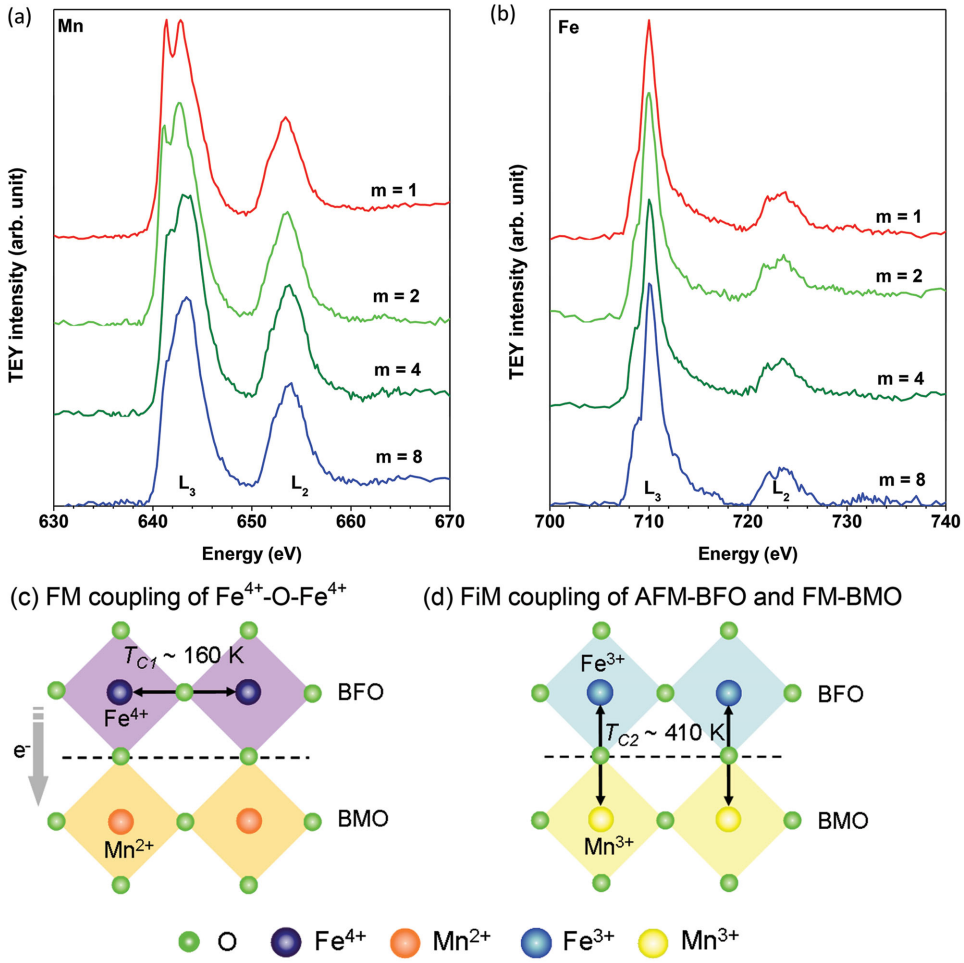

Figure 4. Normalized XAS spectra of SL–BFO/BMO at 300 K in total electron yield (TEY) mode: a) along the Mn $L_{2,3}$ edge and b) along the Fe $L_{2,3}$ edge. Schematic diagram indicating the origin of c) T_{C1} for FM coupling and d) T_{C2} for FiM coupling.

For all our superlattices, we found two magnetic transitions and clear magnetization at temperatures above the T_C of BMO. For the very short period superlattices, m = 1, 2, magnetization was even found above room temperature. Since the change in tetragonal distortion of BMO was minimal and remained above 1, the variation in magnetic behavior is not expected to result from a change in Jahn–Teller distortion.[45] Therefore, to understand the origin of the magnetic states and the enhancement in T_C, we consider the various superexchange interactions between $Fe^{4+/3+}$ and $Mn^{2+/3+}$ that may be present in our m = 1 superlattices, taking the Goodenough–Kanamori (GK) rule into account.[46] First of all, according to these rules, most of the possible interactions are AFM (Fe^{4+}–O–Mn^{3+}, Fe^{3+}–O–Mn^{2+}, Fe^{3+}–O–Fe^{3+}, Mn^{2+}–O–Mn^{2+}, Fe^{4+}–O–Mn^{2+}).[14,46] Also the Fe^{4+}–O–Fe^{3+} interaction can be expected to be AFM as found in $La_{1-x}Sr_xFeO_3$.[47,48] The presence of these AFM interactions may only decrease the total M_S of the superlattices. Therefore, to understand the magnetic behavior of the BMO/BFO superlattices we focus on the remaining interactions, ferromagnetic Mn^{3+}–O–Mn^{3+}, Fe^{4+}–O–Fe^{4+}, and Mn^{2+}–O–Mn^{3+}, and ferri/ferromagnetic Fe^{3+}–O–Mn^{3+}.

First of all, the Mn^{3+}–O–Mn^{3+} interactions present in BMO are likely to be present in the superlattices too. Normally, Mn^{3+}–O–Mn^{3+} interactions give rise to an AFM interaction. However, due to the presence of Bi 6s lone pairs, BMO has 3 dimensional (3D) magnetic structure, leading to FM behavior.[49] For the m = 4, 8 superlattices, we can expect bulk-like BMO to be present. For these superlattices, a clear magnetic transition is present around 100 K, which is close to the T_C of bulk BMO. Therefore, this transition likely originates from the Mn^{3+}–O–Mn^{3+} interactions and is named $T_{C,BMO}$. For the m = 1,2 superlattices, we would expect the Mn^{3+}–O–Mn^{3+} interaction to be mainly in-plane. This also confirms why no clear transition is found around 100 K.

Three dimensional ferromagnetic Fe^{4+}–O–Fe^{4+} interactions are observed in $BaFeO_3$, leading to a T_C of 115 K and a M_S of 3.5 μ_B/Fe.[50] Interestingly, the T_C of $BaFeO_3$, is fairly close to the T_{C1} of our SL–BMO/BFO (140–160 K). Moreover, $BaFeO_3$ shows an enhancement of T_C with increasing unit-cell volume. Interestingly, this trend is similar to the behavior of T_{C1} in our superlattices where the unit cell volume of BFO increases with m as a result of the increase in out-of-plane lattice (Figures 2 and 3c). These similarities strongly suggest that T_{C1} may originate from the FM Fe^{4+}–O–Fe^{4+} interactions. Therefore, let us take a closer look the found magnetic moment for T_{C1}. First of all, the deconvoluted M–T curves with T_{C1} show that magnetic moment increases when decreasing m (see Figure S1c in the Supporting information). This is in agreement with the increase of Fe^{4+} content for lower m. The higher magnetic moment found for m = 2 compared to m = 1 can be explained by the greater 3D character of the Fe^{4+}–O–Fe^{4+} interactions for m = 2. Secondly, M_S is 0.78 μ_B/Fe at 10 K and 5 T from the deconvoluted M–H loop2 (as shown in Figure S2 in the Supporting Information) was found for m = 1, when the magnetic moment would come solely from Fe–Fe interactions. If we assume $\sim^1/_3$ of the Fe ions to be Fe^{4+} in the single layers of BFO, then we may expect a maximum magnetic moment of approximately 1.2 μ_B/Fe for m = 1. However, a magnetic moment of 1.2 μ_B/Fe would mean that Fe^{3+} and Fe^{4+} are fully separated within the layer. As Fe^{3+} and Fe^{4+} in-plane intermixing is expected, the presence of Fe^{3+}–O–Fe^{4+} AFM interactions would reduce the total magnetic moment, explaining the observed M_S of 0.78 μ_B/Fe for m = 1. The resemblance between $BaFeO_3$ and our superlattices, and the observation of Fe^{4+} in the XAS spectra suggest that T_{C1} originates from ferromagnetic Fe^{4+}–O–Fe^{4+} interactions in BFO.[50] The origin of T_{C1} is schematically pictured in Figure 4c.

As mentioned in the introduction, ferromagnetic interactions between AFM BFO and FM BMO are predicted to result in a T_C of ≈406 K for NCB–BFO/BMO.[10] The high T_{C2} of up to 410 K in our very short period SL–BFO/BMO is very close to this predicted T_C. SL–BFO/BMO films have the same lowest energy magnetic ordering as NCB–BFO/BMO: ferrimagnetic ordering of AFM–Fe and FM–Mn (Figure 4c).[10] The absence of T_{C2} for m = 4, 8 superlattices is consistent with the increasing out-of-plane lattice parameter in BFO structure with increasing m, and the separation of BFO and BMO into two distinct lattices (Figures 2 and 3c) rather than a single strain BFO–BMO lattice. Here, the distortions of the BO_6 octahedra at the BMO/BFO interfaces may be not suitable for optimum magnetic coupling.[25–28]

Similar effects of strongly sensitive magnetic properties to structural distortion have been observed previously in superlattices of $[(La_{2/3}Ca_{1/3}MnO_3)_4/(BaTiO_3)_4]_{20}$ (SL–LCMO/BTO) and $[(La_{2/3}Sr_{1/3}MnO_3)_3/(BaTiO_3)_3]_{25}$ (SL–LSMO/BTO). Strong enhancements of T_C were found in these strained superlattices, 1000 K for SL–LCMO/BTO, and 650 K for SL–LSMO/BTO, whereas in relaxed bulk and plain thin films of LCMO and LSMO lower T_Cs of only 250 and 370 K, respectively, were achieved.[25]

Another possibility that we cannot discount for the origin of the high T_{C2} phase in our films is double exchange FM coupling of Mn^{2+}–O–Mn^{3+} in BMO as a clear mixed valence of Mn^{2+} and Mn^{3+} was observed in the m = 1, 2 superlattices (Figure 4a). According to several reports on electron doped $LaMnO_3$, e.g., $La_{1-x}Ce_xMnO_3$, FM ordering with T_C of 250 K has been reported.[46,47] Also, in $La_{1-x}Ce_xMnO_3$ for x up to 0.3, T_C increases as the amount of Mn^{2+} increases. However, the T_C of $La_{1-x}Ce_xMnO_3$ is still much lower than T_{C2} of SL–BFO/BMO. But this could be due to a difference in BO_6 octahedral rotations which has been shown to affect the T_C of LSMO significantly.[26] In addition, this double exchange FM coupling of Mn^{2+}–O–Mn^{3+} should result in metallic behavior below T_{C2} caused by electron hopping, just as for $La_{1-x}Ce_xMnO_3$ with x = 0.3.[51,52] However, independent of m, all our superlattices are highly resistive, which indicates that the Mn^{2+}–O–Mn^{3+} is not the dominant interaction. Therefore, we strongly expect the ferrimagnetic interaction between AFM–BFO and FM–BMO to be the origin of T_{C2}.

In summary, in BFO/BMO superlattices of very high crystalline quality we observed above room temperature magnetic transition temperatures for very short period superlattices. A T_C of 410 K was observed for m = 1, and a T_C of 320 K was observed for m = 2. This T_C phase, T_{C2}, agrees remarkably well to a similarly structured nanoscale checkerboard BFO/BMO lattice, which was shown by theory to have a T_C of 406 K as a result of FM BMO–AFM BFO interactions. A lower T_C, T_{C1}, was observed in all the superlattices (m = 1–8 u.c.) and can be

explained by ferromagnetic Fe^{4+}–O–Fe^{4+} interactions in BFO. Artificial superlattices of ferroelectric BFO and BMO with interface-induced high temperature magnetism are an important prerequisite for creating practical magnetoelectric systems.

Experimental Section

Film Fabrication: BFO_m/BMO_m superlattices (m = 1, 2, 4, 8 u.c.) of ≈50 nm total thickness were grown on (001)-oriented STO substrates by pulsed laser deposition using a KrF laser (λ = 248 nm). Commercial ceramic BFO and BMO targets were ablated at a fluence of 1.6 J/cm^2 and a repetition rate of 2–5 Hz. The substrate to target distance was fixed at 12 cm to ensure a slow growth rate which was needed to maintain coherent growth.[31] During growth the substrate temperature was ≈640 °C and the oxygen pressure was fixed at 100 mTorr. The films were cooled down in 300 Torr O_2 by switching off the heater. To determine the growth rates of BMO and BFO, the thicknesses of single phase BFO and BMO films were calibrated by X-ray reflectivity (XRR). The growth rates, 0.01 Å/pulse for BFO and 0.08 Å/pulse for BMO, were subsequently set to control the fabrication of the superlattices. It was found that the BMO did not grow layer-by-layer which could be expected since the growth is complicated by the highly volatile Bi as well as the large lattice mismatch between pseudocubic BMO and STO.[31] It is noted that the interface roughening of our superlattices increased with film thickness as confirmed by XRR.

Structural Analysis: Structural analyses were carried out by XRR (nonmonochromated Bruker D8 XRD), XRD (Panalytical Empyrean high resolution XRD), and high resolution cross-sectional transmission electron microscopy (TEM, JEOL 4000EX microscope operating at 400 kV).

Magnetic Analysis: Magnetization measurements versus temperature and field (H) were performed using a vibrating sample magnetometer (VSM, Princeton) and a superconducting quantum interference device (SQUID) magnetometer (Quantum Design, MPMS). To investigate the valence state of Fe and Mn in the films, XAS was performed on beamline U4B at the National Synchrotron Light Source (NSLS), Brookhaven National Laboratory. The spectra were measured by total electron yield (TEY) mode at 300 K after pulsing at 9.5 kOe. To prevent charging, silver paste was used at the corner of the sample to create a conducting path.

Supporting Information

Supporting Information is available from the Wiley Online Library or from the author.

Acknowledgements

This research was funded by the Engineering and Physical Sciences Research Council (EP/P50385X/1) and the European Research Council (ERC-2009-AdG 247276 NOVOX). The work at Texas A&M was funded by the US National Science Foundation (DMR-1401266). The work at Los Alamos was supported by the U.S. Department of Energy through the LANL/LDRD program and was performed, in part, at the Center for Integrated Nanotechnologies, a US Department of Energy, Office of Basic Energy Sciences user facility. Use of the National Synchrotron Light Source, Brookhaven National Laboratory, was supported by the US Department of Energy, Office of Science, Office of Basic Energy Sciences, under Contract No. DE-AC02-98CH10886.

Received: September 29, 2015
Revised: November 17, 2015
Published online: January 7, 2016

[1] M. Bibes, A. Barthélémy, *Nat. Mater.* **2008**, *7*, 425.
[2] P. Velev Julian, C.-G. Duan, J. D. Burton, A. Smogunov, M. K. Niranjan, E. Tosatti, S. S. Jaswal, E. Y. Tsymbal, *Nano Lett.* **2009**, *9*, 427.
[3] J. P. Velev, S. S. Jaswal, E. Y. Tsymbal, *Philos. Trans. R. Soc., A.* **2011**, *369*, 3069.
[4] A. A. Belik, *J. Solid State Chem.* **2012**, *195*, 32.
[5] J. R. Teague, R. Gerson, W. J. James, *Solid State Commun.* **1970**, *8*, 1073.
[6] J.-Z. Huang, Y. Shen, M. Li, C.-W. Nan, *J. Appl. Phys.* **2011**, *110*, 094106.
[7] D. I. Khomskii, *J. Magn. Magn. Mater.* **2006**, *306*, 1.
[8] J.-Z. Huang, Y. Wang, Y. Lin, M. Li, C. W. Nan, *J. Appl. Phys.* **2009**, *106*, 063911.
[9] J.-Z. Huang, Y. Shen, M. Li, C.-W. Nan, *J. Appl. Phys.* **2011**, *110*, 094106.
[10] L. Pálová, P. Chandra, K. M. Rabe, *Phys. Rev. B* **2010**, *82*, 075432.
[11] M. T. Anderson, K. B. Greenwood, G. A. Taylor, K. R. Poeppelmeier, *Prog. Solid State Chem.* **1993**, *22*, 197.
[12] A. Ohtomo, S. Chakraverty, H. Mashiko, T. Oshima, M. Kawasaki, *J. Mater. Res.* **2013**, *28*, 689.
[13] P. Mandal, A. Sundaresan, C. N. R. Rao, A. Iyo, P. M. Shirage, Y. Tanaka, Ch. Simon, V. Pralong, O. I. Lebedev, V. Caignaert, B. Raveau, *Phys. Rev. B* **2010**, *82*, 100416.
[14] L. Bi, A. R. Taussig, H.-S. Kim, L. Wang, G. F. Dionne, D. Bono, K. Persson, G. Ceder, C. A. Ross, *Phys. Rev. B* **2008**, *78*, 104106.
[15] D. S. Rana, I. Kawayama, K. Takahashi, K. R. Mavani, H. Murakami, M. Tonouchi, T. Yanagida, H. Tanaka, T. Kawai, *Europhys. Lett.* **2008**, *84*, 67016.
[16] E.-M. Choi, T. Fix, A. Kursumovic, C. J. Kinane, D. Arena, S.-L. Sahonta, Z. Bi, J. Xiong, L. Yan, J.-S. Lee, H. Wang, S. Langridge, Y.-M. Kim, A. Y. Borisevich, I. MacLaren, Q. M. Ramasse, M. G. Blamire, Q. Jia, J. L. MacManus-Driscoll, *Adv. Funct. Mater.* **2014**, *24*, 7478.
[17] M. P. Singh, K. D. Truong, P. Fournier, P. Rauwel, E. Rauwel, L. P. Carignan, D. Ménard, *Appl. Phys. Lett.* **2008**, *92*, 112505.
[18] K. Ueda, H. Tabata, T. Kawai, *Science* **1998**, *280*, 1064.
[19] K. Ueda, H. Tabata, T. Kawai, *Phys. Rev. B* **1999**, *60*, R12561.
[20] K. S. Takahashi, M. Kawasaki, Y. Tokura, *Appl. Phys. Lett.* **2001**, *79*, 1324.
[21] J. W. Freeland, J. Chakhalian, A. V. Boris, J.-M. Tonnerre, J. J. Kavich, P. Yordanov, S. Grenier, P. Zschack, E. Karapetrova, P. Popovich, H. N. Lee, B. Keimer, *Phys. Rev. B* **2010**, *81*, 094414.
[22] A. J. Grutter, H. Yang, B. J. Kirby, M. R. Fitzsimmons, J. A. Aguiar, N. D. Browning, C. A. Jenkins, E. Arenholz, V. V. Mehta, U. S. Alaan, Y. Suzuki, *Phys. Rev. Lett.* **2013**, *111*, 087202.
[23] J. Hoffman, I. C. Tung, B. B. Nelson-Cheeseman, M. Liu, J. W. Freeland, A. Bhattacharya, *Phys. Rev. B* **2013**, *88*, 144411.
[24] M. Gibert, P. Zubko, R. Scherwitzl, J. Íñiguez, J.-M. Triscone, *Nat. Mater.* **2012**, *11*, 195.
[25] A. Sadoc, B. Mercey, C. Simon, D. Grebille, W. Prellier, M.-B. Lepetit, *Phys. Rev. Lett.* **2010**, *104*, 046804.
[26] H. Boschker, J. Kautz, E. P. Houwman, W. Siemons, D. H. A. Blank, M. Huijben, G. Koster, A. Vailionis, G. Rijnders, *Phys. Rev. Lett.* **2012**, *109*, 157207.
[27] J. Hoffman, I. C. Tung, B. B. Nelson-Cheeseman, M. Liu, J. W. Freeland, A. Bhattacharya, *Phys. Rev. B* **2013**, *88*, 144411.
[28] S. J. May, C. R. Smith, J.-W. Kim, E. Karapetrova, A. Bhattacharya, P. J. Ryan, *Phys. Rev. B* **2011**, *83*, 153411.
[29] M. Nakamura, D. Okuyama, J. S. Lee, T. Arima, Y. Wakabayashi, R. Kumai, M. Kawasaki, Y. Tokura, *Adv. Mater.* **2010**, *22*, 500.
[30] Q. Xu, Y. Sheng, M. Khalid, Y. Cao, Y. Wang, X. Qiu, W. Zhang, M. He, S. Wang, S. Zhou, Q. Li, D. Wu, Y. Zhai, W. Liu, P. Wang, Y. B. Xu, J. Du, *Sci. Rep.* **2015**, *5*, 9093.
[31] G. M. De Luca, D. Preziosi, F. Chiarella, R. Di Capua, S. Gariglio, S. Lettieri, M. Salluzzo, *Appl. Phys. Lett.* **2013**, *103*, 062902.
[32] W. Wei, A. Sehirlioglu, *Appl. Phys. Lett.* **2012**, *100*, 071901.

[33] M. Gajek, M. Bibes, A. Barthélémy, K. Bouzehouane, S. Fusil, M. Varela, J. Fontcuberta, A. Fert, *Phys. Rev. B* **2005**, *72*, 020406.
[34] S. Nafis, John A. Woollam, Z. S. Shan, D. J. Sellmyer, *J. Appl. Phys.* **1991**, *70*, 6050.
[35] H.-G. Min, S.-H. Kim, M. Li, J. B. Wedding, G.-C. Wang, *Surf. Sci.* **1998**, *400*, 19.
[36] J. Sort, S. Suriñach, J. S. Muñoz, M. D. Baró, J. Nogués, G. Chouteau, V. Skumryev, G. C. Hadjipanayis, *Phys. Rev. B* **2002**, *65*, 174420.
[37] J. Dho, X. Qi, H. Kim, J. L. MacManus-Driscoll, M. G. Blamire, *Adv. Mater.* **2006**, *18*, 1445.
[38] W. J. Chang, J. Y. Tsai, H.-T. Jeng, J.-Y. Lin, Kenneth Y.-J. Zhang, H. L. Liu, J. M. Lee, J. M. Chen, K. H. Wu, T. M. Uen, Y. S. Gou, J. Y. Juang, *Phys. Rev. B* **2005**, *72*, 132410.
[39] B. Gilbert, B. H. Frazer, A. Belz, P. G. Conrad, K. H. Nealson, D. Haskel, J. C. Lang, G. Srajer, G. De Stasio, *J. Phys. Chem. A* **2003**, *107*, 2839.
[40] H. J. Lee, G. Kim, J.-S. Kang, B. Dabrowski, S. W. Han, S. S. Lee, C. Hwang, M. C. Jung, H. J. Shin, H. G. Lee, J.-Y. Kim, B. I. Min, *J. Appl. Phys.* **2007**, *101*, 09G523.
[41] S. Erat, A. Braun, A. Ovalle, C. Piamonteze, Z. Liu, T. Graule, L. J. Gauckler, *Appl. Phys. Lett.* **2009**, *95*, 174108.
[42] H. Ikeno, I. Tanaka, T. Miyamae, T. Mishima, H. Adachi, K. Ogasawara, *Mater. Trans.* **2004**, *45*, 1414.
[43] S. J. Clark, J. Robertson, *Appl. Phys. Lett.* **2007**, *90*, 132903.
[44] P. Yu, Y. H. Chu, R. Ramesh, *Philos. Trans. R. Soc., A.* **2012**, *370*, 4856.
[45] D. Pesquera, G. Herranz, A. Barla, E. Pellegrin, F. Bondino, E. Magnano, F. Sánchez, J. Fontcuberta, *Nat. Commun.* **2012**, *3*, 1189.
[46] J. B. Goodenough, *Magnetism and the Chemical Bond*, Wiley, New York, USA **1963**.
[47] V. G. Sathe, S. K. Paranjpe, V. Siruguri, A. V. Pimpale, *J. Phys.: Condens. Matter* **1998**, *10*, 4045.
[48] A. Chainani, M. Mathew, D. D. Sarma, *Phys. Rev. B* **1993**, *48*, 14818.
[49] C.-H. Yang, T. Y. Koo, S.-H. Lee, C. Song, K.-B. Lee, Y. H. Jeong, *Europhys. Lett.* **2005**, *74*, 348.
[50] S. Chakraverty, T. Matsuda, N. Ogawa, H. Wadati, E. Ikenaga, M. Kawasaki, Y. Tokura, H. Y. Hwang, *Appl. Phys. Lett.* **2013**, *103*, 142416.
[51] C. Mitra, P. Raychaudhuri, J. John, S. K. Dhar, A. K. Nigam, R. Pinto, *J. Appl. Phys.* **2001**, *89*, 524.
[52] P. Raychaudhuri, C. Mitra, P. D. A. Mann, S. Wirth, *J. Appl. Phys.* **2003**, *93*, 8328.

